



OPEN ACCESS

EDITED BY

Hang Zhou,
Zhejiang University, China

REVIEWED BY

Yao Luo,
Sichuan University, China
Abir Swaidan,
University of California, Los Angeles,
United States

*CORRESPONDENCE

Wei Yang
✉ 13681408183@163.com
Liang Dong
✉ dongliang1983610@163.com

†These authors have contributed equally to this work

RECEIVED 10 October 2025

REVISED 11 December 2025

ACCEPTED 11 December 2025

PUBLISHED 07 January 2026

CITATION

Bai J, Zhang Q, Wang S, Wang H, Yan K, Zhou W, Dong L and Yang W (2026) Multimodal ultrasonography for predicting epidermal growth factor receptor mutation in subpleural non-small cell lung carcinoma. *Front. Oncol.* 15:1722238. doi: 10.3389/fonc.2025.1722238

COPYRIGHT

© 2026 Bai, Zhang, Wang, Wang, Yan, Zhou, Dong and Yang. This is an open-access article distributed under the terms of the [Creative Commons Attribution License \(CC BY\)](https://creativecommons.org/licenses/by/4.0/). The use, distribution or reproduction in other forums is permitted, provided the original author(s) and the copyright owner(s) are credited and that the original publication in this journal is cited, in accordance with accepted academic practice. No use, distribution or reproduction is permitted which does not comply with these terms.

Multimodal ultrasonography for predicting epidermal growth factor receptor mutation in subpleural non-small cell lung carcinoma

Jing Bai^{1†}, Qifei Zhang^{1†}, Song Wang¹, Hong Wang¹, Kun Yan¹, Wei Zhou², Liang Dong^{2*} and Wei Yang^{1*}

¹Key Laboratory of Carcinogenesis and Translational Research (Ministry of Education/Beijing), Department of Ultrasound, Peking University Cancer Hospital & Institute, Beijing, China, ²Department of Ultrasonography, Shengli Oil Field Central Hospital, Dongying, Shandong, China

Objective: Currently precise target treatment based on gene status significantly improved the outcome for patients with non-small cell lung cancer (NSCLC) and epidermal growth factor receptor (EGFR) was the most important gene. We aimed to develop a multimodal ultrasound model for predicting EGFR mutation status in patients with subpleural NSCLC, to provide important information for precise target treatment.

Methods: 75 patients with pathologically confirmed NSCLC were included in this retrospective study. Patients were divided into two groups based on EGFR mutation status: wild-type (n=57) and mutant (n=18). The clinical characteristics (C), conventional ultrasound (US) features, contrast-enhanced ultrasound (CEUS) characteristics, and time-intensity curve (TIC) parameters of the lung lesions were analyzed and compared between the two groups. Univariate and multivariate logistic regression determined independent predictors of EGFR mutations. Two predictive models were constructed: a C+US model and a FULL model. Both were presented using nomograms. Receiver operating characteristic and calibration curves evaluated predictive performance of two models, while decision curve analysis (DCA) assessed clinical utility.

Results: Multivariate analysis identified smoking status, lesion boundaries, and air bronchogram as predictors in the C + US model. The FULL model identified lesion boundaries and air bronchogram on US, enhancement intensity of lesions and internal necrosis on CEUS and RT (rise time) from TIC as predictors. The C + US model achieved an AUC of 0.843, and the FULL model achieved 0.939. DCA confirmed substantial net clinical benefits.

Conclusion: The models developed in this study enabled patients who are unable to undergo invasive procedures to predict EGFR mutation status noninvasively. These findings provided an ultrasound-based diagnostic reference to support clinician decision-making and personalized treatment planning.

KEYWORDS

contrast-enhanced ultrasound, EGFR mutation, non-small cell lung cancer, predictive model, ultrasonography

Introduction

Lung cancer persists as the predominant contributor to global cancer-related morbidity and mortality, with non-small cell lung cancer (NSCLC) constituting approximately 85% of cases (1). Recent advances in molecular biology have identified several driver mutations, including epidermal growth factor receptor (EGFR), BRAF, ROS1, MET, and ALK, which are closely related to the pathogenesis and progression of lung cancer (2). Consequently, targeted therapies have transformed the treatment landscape for individuals with NSCLC (3, 4). Notably, epidermal growth factor receptor tyrosine kinase inhibitors (EGFR-TKIs) are widely administered to individuals harboring EGFR mutations and have been shown to significantly prolong survival (5, 6). The decision to initiate targeted therapy relies on EGFR mutation status evaluation (7) which achieved through pathological examination. However, this process can be limited by the general condition of the patients, biopsy operation ability of the doctors, sample quality and intratumoral heterogeneity (8–11). Therefore, the development of noninvasive methods to predict EGFR mutation status is essential to complement gene sequencing.

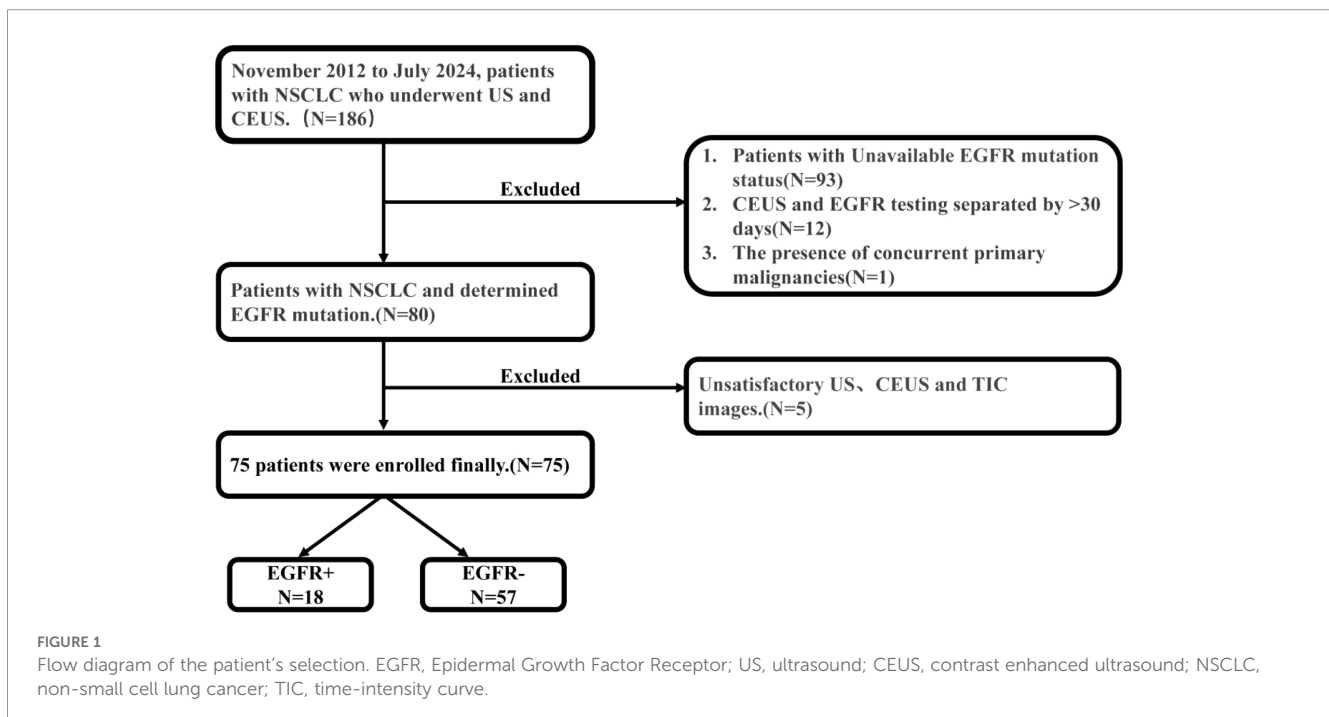
Although CT remains essential in lung cancer imaging, it involves exposure to ionizing radiation (12). In contrast, multimodal ultrasound imaging offers high sensitivity, real-time monitor, and nonionizing advantages in evaluating peripheral lung lesions. Its utility in distinguishing benign from malignant pulmonary lesions and in identifying histological subtypes of lung cancer has been well-proven by our center and other studies (13, 14). Beside the role of characterization of lung lesions with CEUS, we further explored the perspective of CEUS in prediction of gene status which related to target therapy. In this study, we aimed to identify ultrasound (US) and contrast-enhanced ultrasound (CEUS) features associated with

EGFR mutation status and to construct predictive models for assessing EGFR genotype. To our knowledge, this work was the first study to apply ultrasonographic imaging for predicting EGFR mutation status in subpleural non-small cell lung cancer.

Materials and methods

Study design and patients

From November 2012 to July 2024, totally 186 consecutive patients with confirmed peripheral lung NSCLC underwent US and CEUS examination at our department were collected retrospectively. The inclusion criteria were as follows: (i) age ≥ 18 years; (ii) histologically confirmed NSCLC; (iii) documented pretreatment EGFR mutation status; and (iv) availability of pretreatment US and CEUS images. Exclusion criteria were as follows: (i) an interval >1 month between the ultrasound examination and EGFR testing; (ii) the presence of concurrent primary malignancies and (iii) unsatisfactory US, CEUS and TIC images. The final study population included 75 individuals (30 females, 45 males) with an average age of 64.08 ± 11.01 years. All 75 enrolled patients including 47 patients tested by our internal pathology laboratory and 28 cases tested by external laboratories holding equivalent accreditation were tested for EGFR mutations using Amplification refractory mutation system polymerase chain reaction (ARMS-PCR) method. The commercial ADx-EGFR Mutation Detection Kit (AmoyDx) was utilized on the ABI 7500 Real-Time PCR system (Applied Biosystems). This assay is designed to detect 29 somatic mutations in the EGFR gene, including exon 19 deletions, the T790M mutation, and mutations in exons 18, 20, and 21 (such as L858R and L861Q). The patient selection flowchart was illustrated in Figure 1.



Ethical approval

We confirmed that this study adheres to the Declaration of Helsinki. This study was approved by our local ethics committee, and written informed consent was waived because of retrospective study.

CEUS examination methods

The contrast agent was SonoVue (Bracco SpA, Italy). The lyophilized powder was reconstituted with 5 mL of saline to produce a uniform microbubble suspension containing 8 $\mu\text{L}/\text{mL}$ of sulfur hexafluoride encapsulated in a phospholipid shell. A 2.4 mL bolus of the suspension was injected into the antecubital vein over 2–3 s. CEUS images were acquired using the Logiq E9 ultrasound system. The frequency and depth settings used for CEUS were identical to those of conventional US. The mechanical index was adjusted to 0.11–0.13. The timer was activated simultaneously with contrast injection. Lesions were assessed using contrast-enhanced harmonic US with continuous recording for ≥ 180 seconds. Dynamic images were saved to the internal hard drive of the ultrasound system.

Enhancement process were classified as arterial and parenchymal phases, beginning at contrast administration. The arterial phase was defined as the interval from the initial appearance of the contrast agent in the lesion to the point of peak enhancement. Time-intensity curves were generated using the built-in postprocessing software of the Logiq E9 ultrasound equipment.

Evaluation of US, CEUS, and TIC

Two radiologists (W.Y. and J.B.), each with 5–10 years of experience in lung ultrasound and contrast-enhanced ultrasound, independently evaluated the US and CEUS images. They jointly reviewed the imaging data and formulated consensus reports. Both radiologists were blinded to the patients' EGFR mutation status.

In the US assessment, lesion boundaries were classified as well defined or poor defined. Lesion shapes were categorized as suborbicular, irregular, or wedge-shaped. Using surrounding atelectasis normal lung tissue as a reference, echogenicity was defined as hypoechoic or isoechoic. An air bronchogram was defined as a tubular or branching air-filled structure within the tumor, resulting from ultrasound reflections of residual air-filled bronchi with posterior comet-tail artifacts. Pleural retraction was described as inward pleural displacement toward the tumor, attributed to fibrotic contraction within tumor tissue.

In CEUS evaluation, enhancement patterns during the arterial phase were classified as: (i) centripetal perfusion, where contrast agent entered from the periphery toward the center; (ii) eccentric perfusion, where perfusion began on one side of the lesion and extended across; and (iii) disorganized enhancement, where perfusion occurred randomly throughout the lesion. Necrosis types were defined as: (i) type A, no necrosis; (ii) type B, single or

multiple necrotic foci. Hydrothorax was recorded as present or absent. Homogeneity was classified as present or absent based on uniform echo intensity within the lesion, excluding necrotic areas at peak contrast enhancement. Enhancement intensity, relative to adjacent normal lung tissue, was classified as hyperenhancement or hypoenhancement.

The CEUS video was analyzed frame by frame to generate the TIC. The enhancement arrival time (AT) was defined as the interval from contrast injection to the initial enhancement of the lesion. The rise time (RT) was defined as the time from initial enhancement to peak enhancement. The time to peak (TTP) was calculated as the sum of AT and RT. The peak intensity (PI) was defined as the echo intensity at peak enhancement. The wash-in area under the curve (Wi-AUC) represented the area under the TIC during the wash-in phase of contrast enhancement.

Statistical analysis and model development

All statistical analyses were performed using R software (version 4.4.3). The 75 patients were stratified into EGFR mutant and EGFR wild-type groups based on mutation status. Categorical variables were described as frequencies and percentages, while continuous variables were reported as mean \pm standard deviation (SD) or median with range. Categorical variables were compared using the χ^2 test or Fisher's exact test. Continuous variables were analyzed using Student's t-test or the Mann-Whitney U-test, as appropriate. A p-value of <0.05 was considered statistically significant.

Variables showing statistical significance in clinical characteristics, US features, CEUS findings, and TIC parameters were further analyzed using univariate and stepwise multivariate logistic regression. Odds ratios (ORs) were calculated for all variables included in multivariate analysis. Two predictive models and their corresponding nomograms were constructed based on the multivariate logistic regression results. The discriminative performance of models was evaluated through Receiver operating characteristic (ROC). The area under the curve (AUC) was calculated, and the optimal cutoff value was determined using the Youden index. Calibration curves were used to assess model calibration, and decision curve analysis (DCA) evaluated clinical utility.

Results

Clinical characteristics

A total of 75 patients were enrolled in this study. Patients were stratified into an EGFR wild-type group ($n = 57$) and an EGFR-mutant group ($n = 18$) based on EGFR mutation status. The clinical characteristics and corresponding statistical comparisons between the two groups were presented in Table 1. Statistically significant differences between groups were observed in sex ($p = 0.001$) and smoking status ($p < 0.001$). Meanwhile, no significant differences

TABLE 1 Comparison of clinical characteristics of patients with or without EGFR mutation.

Variable	EGFR- (N=57)	EGFR+ (N=18)	<i>p</i>
Age, Mean \pm SD	63.91 \pm 10.13	64.61 \pm 13.78	0.816
Sex, <i>n</i> (%)			0.001**
Female	17 (29.82%)	13 (72.22%)	
Male	40 (70.18%)	5 (27.78%)	
TNM Stage, <i>n</i> (%)			0.312
Available	60 (80.00%)		
I-III	13	2	
IV	31	14	
NA	15 (20.00%)		
Smoking status, <i>n</i> (%)			<0.001***
Former	41 (71.93%)	5 (27.78%)	
Never	16 (28.07%)	13 (72.22%)	
Histological subtype, <i>n</i> (%)			0.133
Adenocarcinomas	40 (70.18%)	16 (88.89%)	
Squamous cell carcinomas	17 (29.82%)	2 (11.11%)	
Tumor location, <i>n</i> (%)			0.861
Left	24 (42.11%)	8 (44.44%)	
Right	33 (57.89%)	10 (55.56%)	
Size, Median (Q1-Q3)	5.72 (4.72-7.55)	6.02 (3.11-8.25)	0.664

EGFR, epidermal growth factor receptor; TNM, tumor node metastasis; NA, not applicable. ***p* < 0.01, ****p* < 0.001. Bold values indicate *p* < 0.05.

were observed in age (*p* = 0.816), TNM stage (*p* = 0.312), histological subtype (*p* = 0.133), tumor location (*p* = 0.861), and tumor size (*p* = 0.664) between EGFR+ and EGFR- groups.

Development of models

The US features, CEUS characteristics, and TIC parameters were summarized in Table 2. Significant differences were identified in US features, including lesion boundaries (*p* = 0.017) and air bronchogram (*p* = 0.012). In CEUS, enhancement pattern (*p* = 0.034), homogeneity (*p* < 0.001), enhancement intensity (*p* = 0.026), and internal necrosis (*p* = 0.011) differed significantly between the two groups. Additionally, there was significant difference in RT on TIC analysis (*p* = 0.015).

The results of univariate logistic regression for all statistically significant parameters were displayed in Table 3. The clinical characteristics (sex, smoking status) and US features (boundaries, air bronchogram) were entered into a stepwise multivariate logistic regression. Smoking status (*p* = 0.003), lesion boundaries (*p* =

0.090) and air bronchogram (*p* = 0.007) were identified as independent predictors. A combined C + US model was constructed using these three variables (Table 4), and its corresponding nomogram was illustrated in Figure 2.

Subsequently, clinical characteristics (sex, smoking status), US features (boundaries, air bronchogram), CEUS characteristics (homogeneity, enhancement intensity, necrosis), and the TIC parameter RT were analyzed via stepwise multivariate logistic regression. Lesion boundaries (*p* = 0.002), air bronchogram (*p* = 0.013), enhancement intensity (*p* = 0.020), internal necrosis (*p* = 0.002), and RT (*p* = 0.008) were identified as independent predictors for EGFR status. Based on these five variables, the FULL model was developed (Table 5), with a corresponding nomogram shown in Figure 3. Figures 4A–C, 5A–C demonstrated ultrasound images and pathological image of EGFR-wild type and EGFR-mutant lesions, respectively.

Performance and validation of two models

The ROC curves for both predictive models were presented in Figure 6. The FULL model demonstrated superior diagnostic performance compared to the C + US model (AUC: 0.939 vs. 0.843, *p* < 0.05). The predictive metrics of both models, including specificity, sensitivity, negative predictive value, positive predictive value, and accuracy were summarized in Table 6. Calibration curves (Figures 7, 8) demonstrated high concordance of predictions with observations in both models. DCA further confirmed the clinical utility of both models. As shown in Figure 9, the FULL model provided greater net clinical benefit than the C + US model across most threshold probabilities. The FULL model demonstrated a substantial improvement in predictive performance compared to the C+US model, attributable to the integration of CEUS features and TIC parameters.

Discussion

Since targeted therapy provides meaningful survival benefits and quality-of-life improvements in advanced lung cancer, accurate detection of EGFR status before treatment is crucial throughout clinical management.

Multiple studies support the predictive value of radiomic features for EGFR genotype in NSCLC (10, 11, 15, 16). Several studies have suggested that female individuals and never-smokers are more likely to harbor EGFR mutations (17–19). Additionally, prior research using computed tomography (CT) and PET/CT imaging has demonstrated that imaging features such as ground-glass opacity, convergence of surrounding vessels, pleural retraction, and adjacent invasion are correlated with EGFR mutation status (20–22). Compared to CT, US, particularly CEUS, offers real-time monitoring, absence of radiation exposure, accessibility, and cost-effectiveness, making it a viable supplemental imaging tool for the differential diagnosis of subpleural pulmonary lesions. Existing studies have confirmed the high sensitivity of US and CEUS in diagnosing pulmonary and pleural lesions and in

TABLE 2 Comparison of US, CEUS and TIC features of lung lesions with or without EGFR mutation.

Variable	EGFR- (N=57)	EGFR+ (N=18)	<i>p</i>
US			
Boundaries, <i>n</i> (%)			0.017*
Well defined	26 (45.61%)	14 (77.78%)	
Poor defined	31 (54.39%)	4 (22.22%)	
Shape, <i>n</i> (%)			0.816
Suborbicular	27 (47.37%)	10 (55.56%)	
Irregular	27 (47.37%)	7 (38.89%)	
Wedge-shaped	3 (5.26%)	1 (5.56%)	
Echo, <i>n</i> (%)			0.567
Hypoecho	55 (96.49%)	17 (94.44%)	
Iso echo	2 (3.51%)	1 (5.56%)	
Air bronchogram, <i>n</i> (%)			0.012*
Yes	19 (33.33%)	12 (66.67%)	
No	38 (66.67%)	6 (33.33%)	
Pleural retraction, <i>n</i> (%)			0.982
Yes	22 (38.60%)	7 (38.89%)	
No	35 (61.41%)	11 (61.11%)	
CEUS			
Enhancement pattern, <i>n</i> (%)			0.034*
Centripetal	37 (64.91%)	12 (66.67%)	
Eccentric	5 (8.77%)	5 (27.78%)	
Disorganized	15 (26.32%)	1 (5.56%)	
Homogeneity, <i>n</i> (%)			<0.001***
Yes	14 (24.56%)	13 (72.22%)	
No	43 (75.44%)	5 (27.78%)	
Enhancement intensity, <i>n</i> (%)			0.026*
Hyperenhancement	24 (42.11%)	13 (72.22%)	
Hypoenhancement	33 (57.89%)	5 (27.78%)	
CEUS washout type, <i>n</i> (%)			0.499
Early washout	48 (84.21%)	14 (77.78%)	
Late washout	9 (15.79%)	4 (22.22%)	
CEUS washout degree, <i>n</i> (%)			0.251
Complete	36 (63.16%)	14 (77.78%)	
Incomplete	21 (36.84%)	4 (22.22%)	
Necrosis, <i>n</i> (%)			0.011*
Yes	41 (71.93%)	7 (38.89%)	
No	16 (28.07%)	11 (61.11%)	
Hydrothorax, <i>n</i> (%)			0.536

(Continued)

TABLE 2 Continued

Variable	EGFR- (N=57)	EGFR+ (N=18)	p
CEUS			
Yes	12 (21.05%)	5 (27.78%)	
No	45 (78.95%)	13 (72.22%)	
TIC			
AT, Mean ± SD	8.96 ± 3.18	8.82 ± 1.85	0.816
RT, Median (IQR)	14.00 (12.00-17.00)	15.46 (15.46-18.75)	0.015*
TTP, Mean ± SD	23.36 ± 5.77	25.47 ± 4.78	0.164
PI, Mean ± SD	20.59 ± 4.19	19.17 ± 4.17	0.216
WiAUC, Mean ± SD	207.80 ± 69.46	235.20 ± 42.98	0.119

TIC, time-intensity curve; AT, Arrive time; RT, Rise time; TTP, Time to peak; PI, Peak intensity; WiAUC, Wash in area under curve. *p < 0.05, ***p < 0.001. Bold values indicate p < 0.05.

TABLE 3 Univariate logistic regression analysis of clinical, US and CEUS features.

Variable	Univariate analysis		
	Beta	OR [95%CI]	p
Sex			
Female	1.81	6.12 [1.98-21.64]	0.003
Male		1 [Reference]	
Smoking status			
Former	-1.90	0.15 [0.042-0.47]	0.002
Never		1 [Reference]	
Boundaries			
Well defined	1.43	4.17 [1.31-16.15]	0.023
Poor defined		1 [Reference]	
Air bronchogram			
Yes	1.39	4.00 [1.34-13.08]	0.016
No		1 [Reference]	
Enhancement pattern			
Centripetal	1.58	4.86 [0.84-92.55]	0.145
Eccentric	2.71	15.00 [1.86-327.36]	0.025
Disorganized		1 [Reference]	
Homogeneity			
Yes	2.08	7.99 [2.54-28.75]	<0.001
No		1 [Reference]	
Enhancement intensity			
Hypoenhancement	-1.27	0.28 [0.08-0.85]	0.031
Hyperenhancement		1 [Reference]	

(Continued)

TABLE 3 Continued

Variable	Univariate analysis		
	Beta	OR [95%CI]	p
Necrosis			
Yes	-1.39	0.25 [0.08-0.74]	0.014
No		1 [Reference]	
RT	0.13	1.14[1.01-1.32]	0.048

C, Clinical characteristics; US, ultrasound; CEUS, contrast enhanced ultrasound; RT, Rise time.

distinguishing benign from malignant pathologies (13). To our knowledge, this is the first study to predict EGFR mutation status in NSCLC with ultrasound. Our findings demonstrated that US enables noninvasive, radiation-free prediction of EGFR status with robust diagnostic performance.

TABLE 4 Stepwise multivariate logistic regression analysis for C+US model.

Variable	Beta	S.E	Z	OR [95%CI]	P
Smoking status					
Former	-2.15	0.72	-2.99	0.12 [0.02-0.44]	0.003
Never				1 [Reference]	
Boundaries					
Well defined	1.21	0.72	1.69	3.36[0.88-15.36]	0.090
Poor defined				1 [Reference]	
Air bronchogram					
Yes	1.95	0.72	2.72	7.02[1.88-32.84]	0.007
No				1 [Reference]	

C, Clinical characteristics; US, ultrasound.

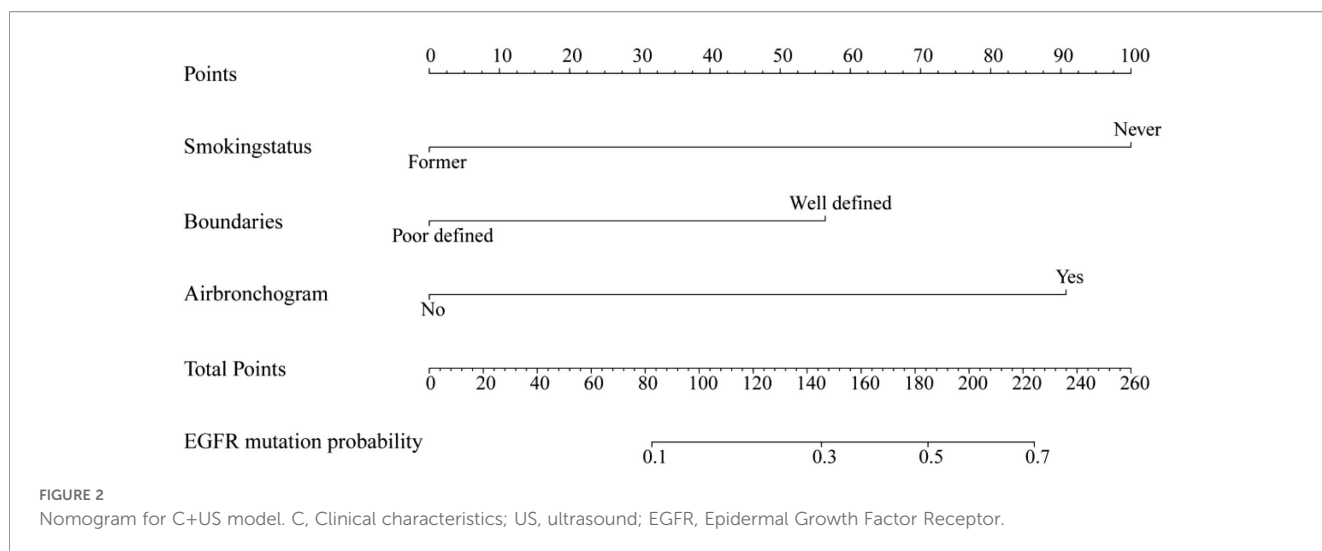


FIGURE 2
Nomogram for C+US model. C, Clinical characteristics; US, ultrasound; EGFR, Epidermal Growth Factor Receptor.

TABLE 5 Stepwise multivariate logistic regression analysis for FULL model.

Variable	Beta	S.E	Z	OR [95%CI]	P
Boundaries					
Well defined	3.58	1.18	3.03	35.99 [4.98-608.62]	0.002
Poor defined				1 [Reference]	
Air bronchogram					
Yes	2.23	0.90	2.48	9.31[1.83-67.96]	0.013
No				1 [Reference]	
Enhancement intensity					
Hypoenhancement	-2.53	1.09	-2.33	0.07[0.01-0.52]	0.020
Hyperenhancement				1 [Reference]	
Necrosis					
Yes	-3.69	1.17	-3.14	0.03 [0.001-0.18]	0.002
No				1 [Reference]	
RT	0.36	0.14	2.64	1.43 [1.13-1.97]	0.008

RT, Rise time.

In our study, univariate analysis revealed a predominance of female and non-smoking patients in the EGFR-mutant group,

consistent with previous studies (10, 11). Prior research has demonstrated that adenocarcinoma is more prone to EGFR mutations. Although our cohort included squamous cell carcinoma cases, no significant association between histologic type and EGFR status was observed, possibly due to the relatively small sample size (23). In the US results, well defined boundaries and air bronchograms were exhibited predominantly in the EGFR-mutant group. This imaging phenotype may relate to the lepidic and expansile growth patterns linked to EGFR mutations. Preserved bronchial structure and air-filled spaces enable bronchogram formation, while the expansile growth pattern likely contributes to well-defined tumor boundaries (20). Regarding CEUS findings, lesions with EGFR mutations were more likely to exhibit homogeneous hyperenhancement and lack necrosis. This imaging phenomenon may reflect EGFR downstream signaling. EGFR mutations activate PI3K-AKT-mTOR pathways, upregulating hypoxia-inducible factor-1 (HIF-1), which promotes vascular endothelial growth factor (VEGF) production. VEGF induces neovascularization by influencing endothelial cells in existing vessels and promoting their migration. The development of abnormal vasculature promotes tumor growth and metastasis. Enhanced vascularization may explain the observed homogeneous hyperenhancement and reduced necrosis (24, 25).

Our study had several limitations. First, the relatively small sample size and limited number of EGFR-mutant events may compromise the stability of the multivariable model and restrict its generalizability to broader populations. Therefore, the model is

TABLE 6 Predictive performance of two models.

Model	AUC	Sensitivity (%)	Specificity (%)	Positive predictive value	Negative predictive value	Accuracy
C+US	0.843	83.3	70.2	73.7	80.8	76.8
FULL	0.939	94.4	86.0	87.1	93.9	90.2

C, Clinical characteristics; US, ultrasound.

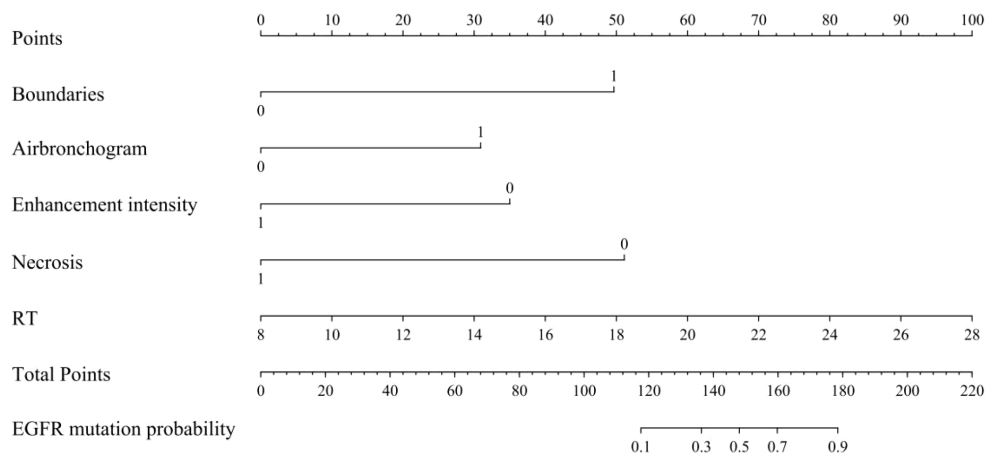


FIGURE 3
Nomogram for the FULL model. RT, rise time; EGFR, Epidermal Growth Factor Receptor.

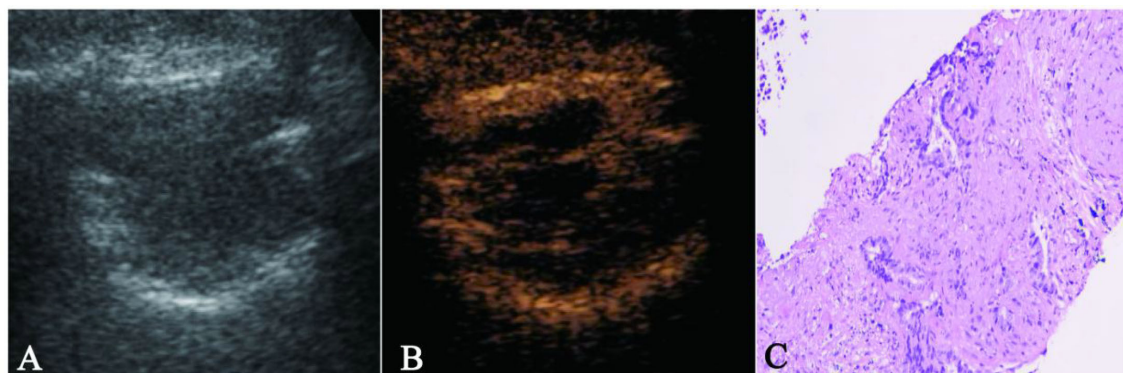


FIGURE 4
The figure 4A–4C showed a case of 70-year-old male NSCLC with EGFR-wild type. (A) The gray-scale ultrasound shown a hypo-echoic lesion with poor defined boundary. (B) On the contrast-enhanced ultrasound, the lesion exhibited hypo-enhancement with multiple necrotic foci. (C) The pathological image confirmed the lesion as a NSCLC.

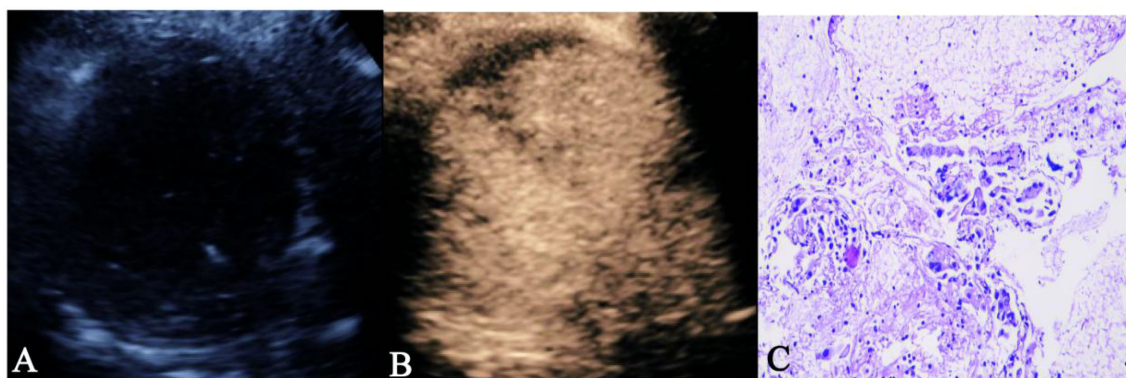


FIGURE 5
The 5A–C showed a case of 50-year-old female NSCLC with EGFR-mutant. (A) The gray-scale ultrasound shown a hypo-echoic lesion with well defined boundary and air bronchograms. (B) On the contrast-enhanced ultrasound, the lesion exhibited homogeneous hyperenhancement. (C) The pathological image confirmed the lesion as a NSCLC.

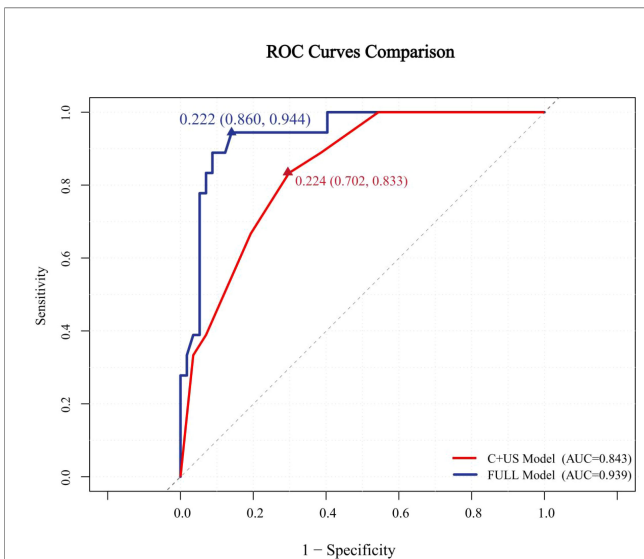


FIGURE 6 Receiver operating characteristic (ROC) curves of the two models with AUC of 0.843 and 0.939. C, Clinical characteristics; US, ultrasound.

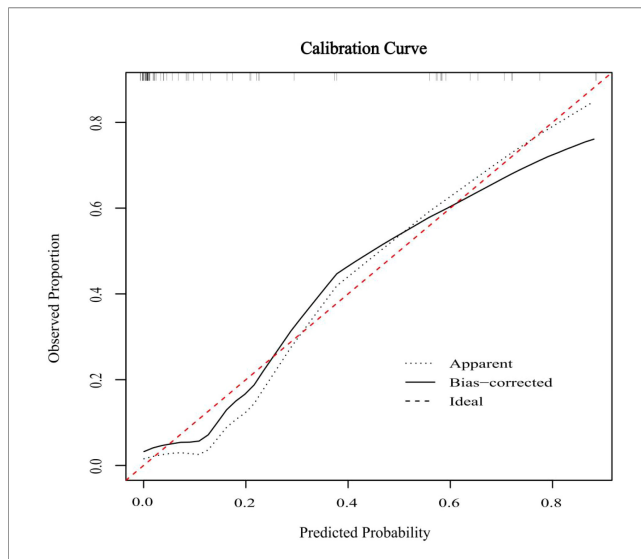


FIGURE 8 Calibration curves of FULL model. C, Clinical characteristics; US, ultrasound; CEUS, contrast enhanced ultrasound; NSCLC, non-small cell lung cancer; TIC, time-intensity curve.

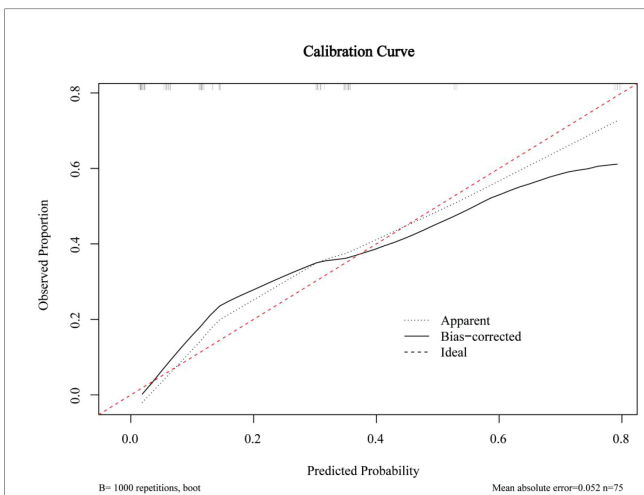


FIGURE 7 Calibration curves of C+US model. C, Clinical characteristics; US, ultrasound.

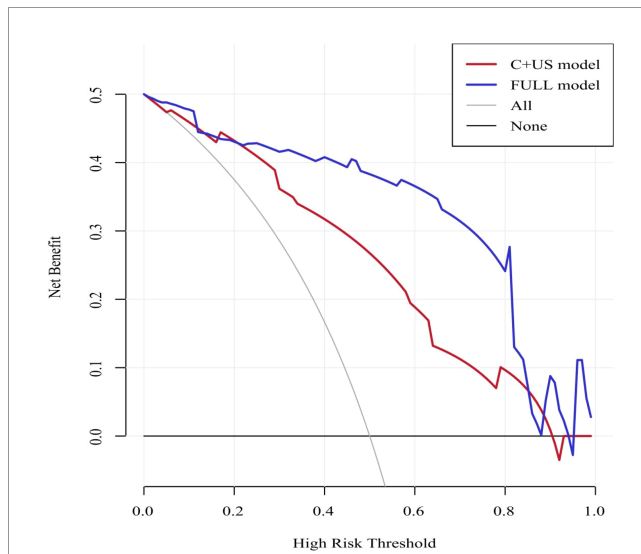


FIGURE 9 Decision curve analysis showing the net clinical benefit of the two models. C, Clinical characteristics; US, ultrasound; NSCLC, non-small cell lung cancer.

exploratory and we will further confirm the results with large samples in multiple centers in the next study. Second, the long study period (2012–2024) introduces the potential of temporal bias, as clinical management, EGFR testing techniques, and ultrasound/CEUS equipment and protocols may have evolved over time. Because the EGFR testing became popular for lung cancer patients in the recent years, we believe we can collect more data during short term period in the future. Third, beyond EGFR, other driver mutations are also relevant to targeted therapy, which need further investigate in the future.

Conclusions

The models developed in this study enable patients who are unable to undergo invasive procedures to predict EGFR mutation status noninvasively. These findings provided an ultrasound-based diagnostic reference to support clinician decision-making and personalized treatment planning.

Data availability statement

The original contributions presented in the study are included in the article/supplementary material. Further inquiries can be directed to the corresponding authors.

Ethics statement

The studies involving humans were approved by Institutional Review Board of the Peking University School of Oncology. The studies were conducted in accordance with the local legislation and institutional requirements. Written informed consent for participation was not required from the participants or the participants' legal guardians/next of kin in accordance with the national legislation and institutional requirements.

Author contributions

JB: Writing – original draft, Writing – review & editing. QZ: Writing – original draft, Writing – review & editing. SW: Software, Writing – original draft. HW: Investigation, Conceptualization, Writing – original draft. KY: Data curation, Methodology, Supervision, Writing – original draft. WZ: Writing – original draft, Project administration, Formal analysis. LD: Writing – original draft, Validation, Project administration. WY: Writing – original draft, Methodology, Writing – review & editing.

Funding

The author(s) declared that financial support was received for this work and/or its publication. This work was supported by national natural science foundation of China (82472002), Capital

References

- Bray F, Laversanne M, Sung H, Ferlay J, Siegel RL, Soerjomataram I, et al. Global cancer statistics 2022: GLOBOCAN estimates of incidence and mortality worldwide for 36 cancers in 185 countries. *CA Cancer J Clin.* (2024) 74:229–63. doi: 10.3322/caac.21834
- Li T, Kung HJ, Mack PC, Gandara DR. Genotyping and genomic profiling of non-small-cell lung cancer: Implications for current and future therapies. *J Clin Oncol.* (2013) 31:1039–49. doi: 10.1200/JCO.2012.45.3753
- Kris MG, Johnson BE, Berry LD, Kwiatkowski DJ, Iafrate AJ, Wistuba II, et al. Using multiplexed assays of oncogenic drivers in lung cancers to select targeted drugs. *JAMA.* (2014) 311:1998–2006. doi: 10.1001/jama.2014.3741
- Lim SM, Kim EY, Kim HR, Ali SM, Greenbowe JR, Shim HS, et al. Genomic profiling of lung adenocarcinoma patients reveals therapeutic targets and confers clinical benefit when standard molecular testing is negative. *Oncotarget.* (2016) 7:24172–8. doi: 10.18632/oncotarget.8138
- An N, Zhang Y, Niu H, Li Z, Cai J, Zhao Q, et al. EGFR-TKIs versus taxanes agents in therapy for non-small-cell lung cancer patients. *Med (Baltimore).* (2016) 95:e5353. doi: 10.1097/MD.0000000000005601
- Hou J, Li H, Ma S, He Z, Yang S, Hao L, et al. EGFR exon 20 insertion mutations in advanced non-small-cell lung cancer: current status and perspectives. *biomark Res.* (2022) 10:21. doi: 10.1186/s40364-022-00372-6
- Lindeman NI, Cagle PT, Aisner DL, Arcila ME, Beasley MB, Bernicker EH, et al. Updated molecular testing guideline for the selection of lung cancer patients for treatment with targeted tyrosine kinase inhibitors. *J Mol Diagn.* (2018) 20:129–59. doi: 10.1016/j.jmoldx.2017.11.004
- Guo L, Chen Z, Xu C, Zhang X, Yan H, Su J, et al. Intratumoral heterogeneity of EGFR-activating mutations in advanced NSCLC patients at the single-cell level. *BMC Cancer.* (2019) 19:847. doi: 10.1186/s12885-019-5555-y
- Mu W, Jiang L, Zhang J, Shi Y, Gray JE, Tunali I, et al. Non-invasive decision support for NSCLC treatment using PET/CT radiomics. *Nat Commun.* (2020) 11:5228. doi: 10.1038/s41467-020-19116-x
- Wang S, Shi J, Ye Z, Dong D, Yu D, Zhou M, et al. Predicting EGFR mutation status in lung adenocarcinoma on computed tomography image using deep learning. *Eur Respir J.* (2019) 53:1800986. doi: 10.1183/13993003.00986-2018
- Hasegawa M, Sakai F, Ishikawa R, Kimura F, Ishida H, Kobayashi K. CT features of EGFR-mutated adenocarcinoma of the lung: Comparison with nonmutated adenocarcinoma. *J Thorac Oncol.* (2016) 11:819–26. doi: 10.1016/j.jtho.2016.02.010
- Smith-Bindman R, Chu PW, Azman FH, Stewart C, Malekheaday M, Alber S, et al. Projected lifetime cancer risks from current computed tomography imaging. *JAMA Intern Med.* (2025) 185:1–8. doi: 10.1001/jamainternmed.2025.0505
- Bai J, Du YQ, Yang W, Bai XM, Wang S, Wu W, et al. The role of contrast-enhanced ultrasound plus color parametric imaging in the differential diagnosis of subpleural pulmonary lesions. *J Ultrasound Med.* (2023) 42:2777–89. doi: 10.1002/jum.16316
- Yu QD, Jing B, Bing W, Song W, Fei ZQ, Kun Y, et al. Differential diagnosis of pathological type of peripheral lung cancer with multimodal contrast-enhanced ultrasound. *Ultrasound Med Biol.* (2024) 50:1485–93. doi: 10.1016/j.ultrasmedbio.2024.05.017

Medical Development Program (2024-2-2157) and Dongying City Major Special Project for Scientific and Technological Innovation (2024ZDJH88).

Conflict of interest

The author(s) declared that this work was conducted in the absence of any commercial or financial relationships that could be construed as a potential conflict of interest.

Generative AI statement

The author(s) declared that generative AI was not used in the creation of this manuscript.

Any alternative text (alt text) provided alongside figures in this article has been generated by Frontiers with the support of artificial intelligence and reasonable efforts have been made to ensure accuracy, including review by the authors wherever possible. If you identify any issues, please contact us.

Publisher's note

All claims expressed in this article are solely those of the authors and do not necessarily represent those of their affiliated organizations, or those of the publisher, the editors and the reviewers. Any product that may be evaluated in this article, or claim that may be made by its manufacturer, is not guaranteed or endorsed by the publisher.

15. Mahajan A, Kania V, Agarwal U, Ashtekar R, Shukla S, Patil VM, et al. Deep-learning-based predictive imaging biomarker model for EGFR mutation status in non-small cell lung cancer from CT imaging. *Cancers (Basel)*. (2024) 16:1123. doi: 10.3390/cancers16061130
16. Zhang J, Zhao X, Zhao Y, Zhang J, Zhang Z, Wang J, et al. Value of pre-therapy 18F-FDG PET/CT radiomics in predicting EGFR mutation status in patients with non-small cell lung cancer. *Eur J Nucl Med Mol Imaging*. (2019) 47:1137–46. doi: 10.1007/s00259-019-04592-1
17. Dogan S, Shen R, Ang DC, Johnson ML, D'Angelo SP, Paik PK, et al. Molecular epidemiology of EGFR and KRAS mutations in 3,026 lung adenocarcinomas: Higher susceptibility of women to smoking-related KRAS-mutant cancers. *Clin Cancer Res*. (2012) 18:6169–77. doi: 10.1158/1078-0432.CCR-11-3265
18. Shi Y, Au JS, Thongprasert S, Srinivasan S, Tsai CM, Khoa MT, et al. A prospective, molecular epidemiology study of EGFR mutations in Asian patients with advanced non-small-cell lung cancer of adenocarcinoma histology (PIONEER). *J Thorac Oncol*. (2014) 9:154–62. doi: 10.1097/JTO.0000000000000033
19. Soria JC, Ohe Y, Vansteenkiste J, Reungwetwattana T, Chewaskulyong B, Lee KH, et al. Osimertinib in untreated EGFR-mutated advanced non-small-cell lung cancer. *N Engl J Med*. (2018) 378:113–25. doi: 10.1056/NEJMoa1713137
20. Zhang H, Cai W, Wang Y, Liao M, Tian S. CT and clinical characteristics that predict risk of EGFR mutation in non-small cell lung cancer: a systematic review and meta-analysis. *Int J Clin Oncol*. (2019) 24:649–59. doi: 10.1007/s10147-019-01403-3
21. Zhu P, Xu XJ, Zhang MM, Fan SF. High-resolution computed tomography findings independently predict EGFR mutation status in ground-glass nodular lung adenocarcinoma. *World J Clin Cases*. (2021) 9:9792–803. doi: 10.12998/wjcc.v9.i32.9792
22. Wang S, Yu H, Gan Y, Wu Z, Li E, Li X, et al. Mining whole-lung information by artificial intelligence for predicting EGFR genotype and targeted therapy response in lung cancer: a multicohort study. *Lancet Digit Health*. (2022) 4:e309–19. doi: 10.1016/S2589-7500(22)00024-3
23. Warth A, Penzel R, Lindenmaier H, Brandt R, Stenzinger A, Herpel E, et al. EGFR, KRAS, BRAF and ALK gene alterations in lung adenocarcinomas: patient outcome, interplay with morphology and immunophenotype. *Eur Respir J*. (2014) 43:872–83. doi: 10.1183/09031936.00018013
24. Sharma M, Basu DA, Nathany S, Amrith BP, Batra U. A narrative review of the role of common EGFR mutations in pathogenesis and treatment of non-small-cell lung carcinoma. *Cancer Res Stat Treat*. (2022) 5:507–18. doi: 10.4103/crst.crst_222_22
25. Wang Q, Zeng A, Zhu M, Song L. Dual inhibition of EGFR-VEGF: an effective approach to the treatment of advanced non-small cell lung cancer with EGFR mutation. *Int J Oncol*. (2023) 62:45–53. doi: 10.3892/ijo.2023.5474